Computers & Fluids 51 (2011) 136–144

Contents lists available at SciVerse ScienceDirect

Computers & Fluids

journal homepage: www.elsevier.com/locate/compfluid

Two-dimensional side-by-side circular cylinders at moderate Reynolds numbers

Ali Vakil, Sheldon I. Green *

Department of Mechanical Engineering, University of British Columbia, Vancouver, BC, Canada

ARTICLE INFO

Article history:
Received 6 August 2010
Received in revised form 13 April 2011
Accepted 8 August 2011
Available online 28 August 2011

Keywords:
Side-by-side cylinders
Drag coefficient
Drag reduction
Wake interaction
Papermaking

ABSTRACT

In a companion article [1], we described computer simulations of the flow around 2 two-dimensional, tandem circular cylinders in a flow for $1 \leqslant Re \leqslant 20$. In this article we adopt a similar approach to characterize the flow around side-by-side cylinders with surface-to-surface separation/diameter in the range $0.1 < s/D < 30$. The results revealed some distinct and interesting features of the flow, which are completely different than those observed at higher Reynolds numbers.

At low Reynolds numbers, $1 \leqslant Re \leqslant 5$, for all gap spacings, the flow contains no regions of flow separation. At higher Re, four distinct flow behaviors were observed. For very small gap spacings, e.g. $0.1 < s/D < 0.6$ at $Re = 20$, two elongated "detached vortices" form downstream of the cylinders. The drag coefficient increases sharply with the gap spacing. For gap spacings $0.6 < s/D < 0.7$ at $Re = 20$, no vortices form anywhere in the flow. For gap spacings around $s/D \approx 1$ separation regions form only on the inside portions of the cylinders. For larger gap spacings $s/D > 1$ the flow reverts to something similar to that around an isolated cylinder in the flow, i.e. two attached vortices on the rear side of each cylinder. In general, the drag coefficient increases as the gap spacing increases. At higher Reynolds number it is known that the cylinder lift coefficients decrease monotonically with gap spacing. In contrast, at these lower Reynolds number the lift coefficient curves rise to a maximum for $0.3 < s/D < 3$ and then decrease monotonically for larger s/D.

1. Introduction

The flow around two or a cluster of cylinders with different orientations is of interest to different fields of engineering, such as the wind flow around the chimneys of a power plant, transmission lines, and struts of a biplane wing, or the flow past columns of a marine structure in offshore engineering [2]. These flows, which generally occur at high Reynolds numbers, are characterized by the wake of the upstream cylinder strongly influencing the downstream cylinder [3].

In contrast with these high Reynolds number interactions, in papermaking lower Re interactions are important. For example, wood fibers, which are approximately cylindrical structures 1 mm long and 40 μm in diameter, often settle in close proximity of one another [4]. An idealization of the settling of two side-by-side wood fibers is the flow over tandem cylinders at low Reynolds numbers (Fig. 1).

Taneda performed experimental studies on the lift of two side-by-side cylinders at Reynolds numbers from 0.01 to 1.6 [5]. He observed that the lift coefficient first increased with increasing separation and then decreased monotonically at larger separation distances. Moreover, the lift coefficient decreased monotonically as the Reynolds numbers increased. His findings were in agreement with the theoretical work by Fujikawa [6]. For a very small Reynolds number (1.1×10^{-2}) no flow separation was observed at $g = s/D = 0.2$, where s is the surface-to-surface gap spacing between the cylinders and d is the cylinders' diameter [7]. Umemura [8] performed a matched-asymptotic analysis of the low Reynolds number flow past a pair of circular cylinders. His results were in fairly good agreement with Taneda's experimental data.

Zdravkovich [9] made a survey of the steady flow interference between two circular cylinders in various arrangements at large Reynolds numbers ($Re \approx 10^5$). He sketched three distinct flow regimes depending on the gap spacing: (1) one single vortex street when the cylinders are close to each other, i.e. $0 < s/D < 0.1 - 0.2$, (2) bistable biased gap flow in the gap spacing range $0.1 - 0.2 < s/D < 1 - 1.2$, (3) coupled vortex streets for $1 - 1.2 < s/D < 4 - 5$. The wakes of the two cylinders were essentially independent when the gap spacing was greater than 5 diameters. A remarkable feature of the flow is the bistable biased gap flow for intermediate cylinder spacings. In biased gap flow, a narrow wake exists behind one cylinder and a wide wake behind the other (it is bistable in the sense that which cylinder has the narrow wake is a function of very slight variations in the approach flow or cylinder geometry). It is surprising that in an entirely symmetrical oncoming flow, the two identical side-by-side cylinders produce an asymmetrical wake. The origin

* Corresponding author. Address: Department of Mechanical Engineering, University of British Columbia, 6250 Applied Science Lane, Vancouver, BC, Canada V6T 1Z4. Tel.: +1 604 822 5562; fax: +1 604 822 2403.

E-mail addresses: alivakil@interchange.ubc.ca (A. Vakil), green@mech.ubc.ca (S.I. Green).

0045-7930/$ - see front matter © 2011 Elsevier Ltd. All rights reserved.
doi:10.1016/j.compfluid.2011.08.008

Nomenclature

C_D	drag coefficient of the cylinders, $C_D = \frac{F_D}{\frac{1}{2}\rho U_\infty^2 D}$
C_L	lift coefficient of the cylinders, $C_L = \frac{F_L}{\frac{1}{2}\rho U_\infty^2 D}$
d_1, d_2, d_3, d_4, d_5	parameters used in C_D curve fit
D	cylinder diameter (m)
H	overall height of geometry (m)
l_1, l_2, l_3, l_4, l_5	parameters used in C_L curve fit
L_{down}, L_{up}, W	computational domain sizes (m)
L_{SB}	cylinders' separation bubble length (m)
Re	Reynolds number based on cylinder diameter
Re_H	Reynolds number based on height normal to the flow
s	surface-to-surface gap spacing between cylinders (m)
S	center-to-center gap spacing between cylinders (m)
U_∞	free stream velocity (m/s)
x	downstream distance (m)
y	distance in the transverse direction (m)
θ_f	forward stagnation point angular position (degrees)
θ_r	rear stagnation point angular position (degrees)
μ	dynamic viscosity (Pa s)
ρ	density (kg/m^3)

of biased gap flow has been discussed in [3,10–12], but no general consensus has been achieved. Bearman and Wadcock [11] have also observed biased gap flow for two side-by-side plates. Hence, they ruled out the hypothesis that the variable position of boundary-layer separation is the reason for the biased flow.

Zdravkovich [9] compiled lift and drag coefficients in side-by-side arrangements in the Reynolds number range $10^3 < Re < 10^5$. As the gap spacing between the cylinders increases the lift coefficient decreases monotonically. In general, at very small separations, the drag of a pair of cylinders is greater than the summation of the drags of the two cylinders in isolation [11]. As the gap spacing increases, the drag coefficient first decreases until the gap spacing is in the range $0.5 \leqslant s/D \leqslant 1$. As the gap size increases further, one of two trends were observed, depending on the Reynolds number: (i) the drag increases monotonically to the value for an isolated cylinder, e.g. at $Re = 6 \times 10^4$ and (ii) it increases to values above that of an isolated cylinder, reaches a maximum, and then asymptotically approaches that of an isolated cylinder, e.g. at $Re = 1.6 \times 10^5$.

For a single two-dimensional cylinder in a uniform flow the laminar Karman vortex street appears for $Re > 40$, and the wake becomes transitional for $Re > 200$. Some new types of periodic vortex shedding and transition between different types have been classified for finite cylinders for $40 < Re < 300$ [13–16]. Two side-by-side cylinders exhibit different shedding patterns and transitional wakes depending on the proximity of the cylinders and the Reynolds number. The biased gap flow present at high Reynolds numbers has also been observed at low Reynolds numbers, e.g. at $Re = 55$ and $s/D = 1$ [17]. For gap spacings $1 < s/D < 5$, Williamson [17] observed that the cylinders shed stable vortices predominantly in antiphase, leading to two antiphase streets. In contrast with the stable out-of-phase shedding, the in-phase vortex shedding between side-by-side cylinders, at gap sizes $s/D < 3$, is not stable and evolves into a large-scale single wake [18–21]. In other words, eddies shed from the inner side of the cylinders roll up and pair with eddies on the outer side forming a "binary eddy street". The stability of the coupled wakes of cylinders in (s/D, Re) space is studied in [22].

In this article we describe numerical simulations of the flow around 2 two-dimensional side-by-side circular cylinders with gap spacings $0.1 < s/D < 30$, and Reynolds numbers between 1 and 20. In Section 2, we describe the numerical method and computational domain used for simulations. Section 3 discusses the results and Section 4 is comprised of a summary and conclusions.

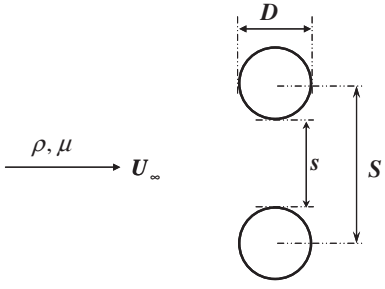

Fig. 1. The geometry of the problem.

2. Numerical method

2.1. Meshing and boundary conditions

The flow around two side-by-side circular cylinders with gap spacing in the range $0.1 < s/D < 30$ was simulated in a typical computational domain shown in Fig. 2. The normal computational domain size was roughly $L_{up} = 250D$, $L_{down} = 500D$ and $W = 500D$. At lower Reynolds numbers, the domain size was increased up to four times relative to the reference domain, but negligible changes in the drag coefficient results were observed. For higher separations between the cylinders, domain sizes were also increased according to the gap spacing.

The lateral walls were considered as zero-shear walls to minimize their effect on the flow. Velocity inlet and pressure outlet boundary conditions were chosen, respectively, for the inlet and outlet of the domains. In the areas close to the cylinders, a boundary layer mesh was used over the cylinder surface and the rest of the domain was meshed with unstructured elements. Fig. 3 depicts a close-up view of the mesh around the cylinders.

The meshed geometry was then imported into the CFD package Fluent™. Owing to the low to moderate Reynolds numbers of interest here, the laminar viscous model in Fluent was used, resulting in

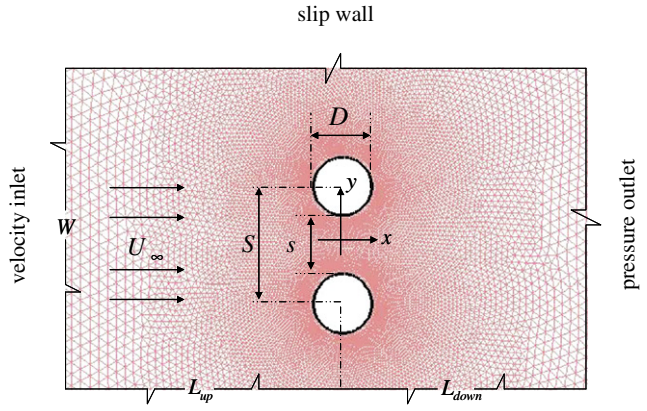

Fig. 2. Computational domain indicating the inlet, outlet, and slip walls. For clarity, not all mesh elements are shown.

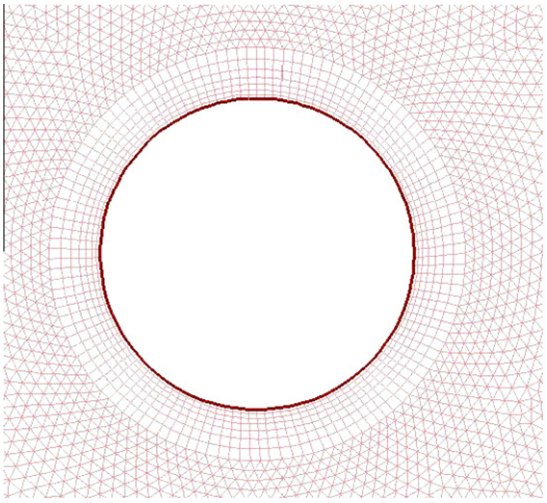

Fig. 3. A close-up view of the hybrid mesh around the cylinders.

a direct numerical simulation of the flow. All simulations were run under steady flow conditions. For spatial discretization, second-order upwinding was used. The SIMPLE scheme was employed for the pressure–velocity coupling. We ran some simulations for Re = 20 with both the steady and unsteady solvers within Fluent. The time-averaged drag coefficients were all within 1% of the steady drag coefficients. No Karman vortex shedding was observed for the unsteady simulations.

2.2. Mesh Independence

To ensure that the simulation results are mesh independent, several flows were simulated with different mesh densities. Two typical cases are shown in Fig. 4. For all flows simulated the drag (lift) coefficient computed with 0.08 million cells was within 0.01% (0.1%) of that computed with a finer mesh. Therefore, the number of cells used in all other cases was between 0.08 and 0.15 million. In general, a larger number of cells were required to achieve mesh independence at low Reynolds numbers owing to the larger domain size that is required to minimize side/end-wall influence.

The pressure distributions over the cylinder surface from the simulations were also compared with those given by Fornberg [24]. The maximum error at Re = 40 was around 1.5%, which occurred at the front stagnation point. The error may be attributed in large measure to digitizing Fornberg's graphs, although numerical dissipation caused by the second-order upwinding used in the momentum equation discretization, which would be most pronounced at this location, likely also played a role.

Table 1
Comparison of drag coefficient between simulations and those in [24,25].

Re	Simulation	Ref. [24]	Difference (%)	Ref. [25]	Difference (%)
20	1.9980	2.0001 ± 0.0002	−0.1	2.0243	−1
40	1.4996	1.4980 ± 0.0005	0.1	1.5075	0.5

A comparison of drag coefficients between our simulations and those reported in [24,25] is given in Table 1. There is excellent agreement between the simulations and the previous studies.

3. Results and discussion

3.1. Flow visualization

3.1.1. Flow definitions

In Section 3.1.2 we describe the flow streamlines as the Reynolds number and the gap spacing are varied. At different values of Re and s/D the flow has distinct and interesting streamlines (Fig. 8), many of which include flow separation. For clarity, we define here some features of the flow. Figs. 5a and b show, respectively, streamlines for an isolated cylinder and for two side-by-side cylinders in the flow. For the single cylinder the separation bubble length, L_{SB}, is the distance between the rear of the cylinder and the stagnation point at the aft of the counter-rotating vortices. For the flow shown in Fig. 5b the flow does not separate on the cylinders' surfaces, but rather separates some distance downstream of the cylinders. For this case, the separation bubble length is defined to be the distance between the forward and aft stagnation points of the vortex pair.

As the gap spacing changes between the cylinders, a number of changes occur in the separation and stagnation points. Before we explain the general behaviors of these points, we first present two typical cases.

Fig. 6a shows the flow at Re = 20 around nearly touching cylinders, $s/D = 0.05$, with the stagnation points labeled on it. For a single isolated cylinder in the flow the front (rear) stagnation point happens at $\theta_f = 90^\circ$ ($\theta_r = 90^\circ$), whereas the proximity of the cylinders moves the front stagnation point to $\theta_f \approx 47^\circ$ and the rear stagnation point to $\theta_r \approx 142^\circ$.

Fig. 6b shows the upper cylinder in the side-by-side configuration with $s/D = 1$ at Re = 20 (a close-up view of Fig. 8(b6)). The singular points for this special gap spacing are different than those of the previous narrow-gap regime. The front stagnation point has moved forward to $\theta_f = 77^\circ$, the rear stagnation point has remained in about the same location, and a separation region has been formed on the inner side of the cylinders.

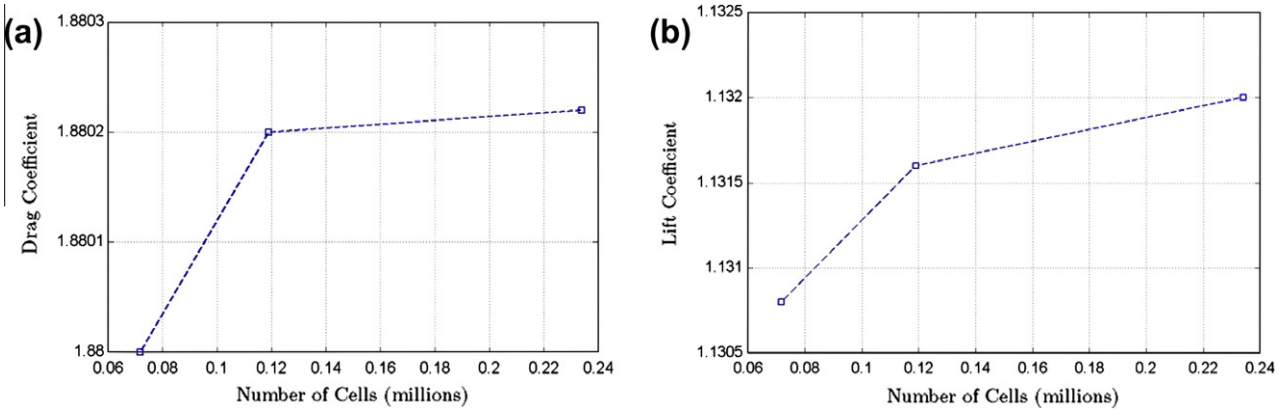

Fig. 4. (a) Drag coefficient and (b) lift coefficient versus number of mesh volumes for $s/D = 0.5$ for Re = 20. Note the highly expanded ordinate axes.

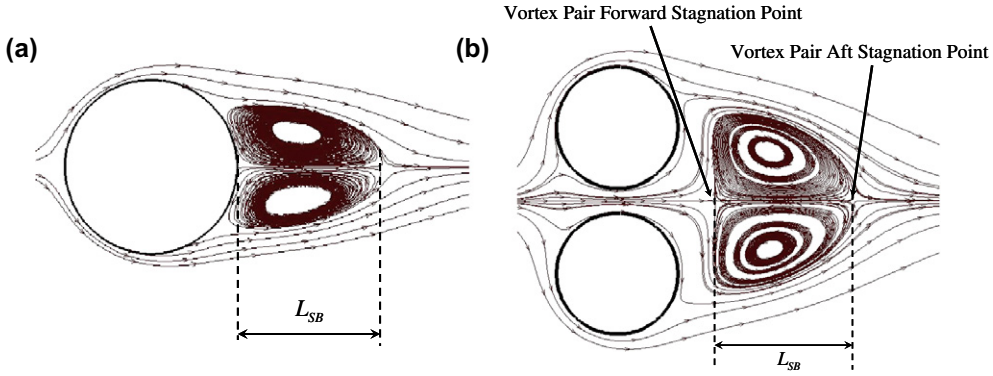

Fig. 5. The definition of the "separation bubble length" for (a) the flow around an isolated cylinder at Re = 20 and (b) the flow around two side-by-side cylinders at Re = 5 and $s/D = 0.2$, showing the "vortex pair forward stagnation point" and "vortex pair aft stagnation point".

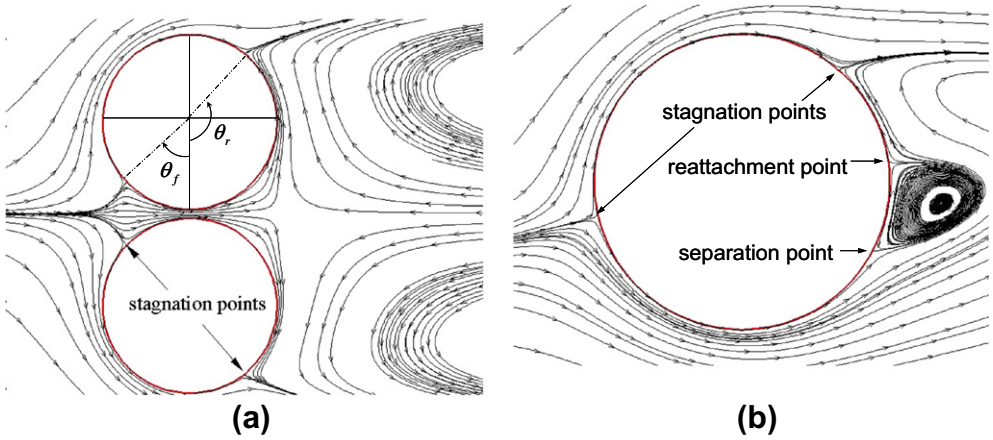

Fig. 6. Close-up view of the flow streamlines showing the stagnation, separation, and reattachment points at (a) Re = 20 and $s/D = 0.05$ and (b) Re = 20 and $s/D = 1$.

3.1.2. Flow characteristics

We start our discussions by considering the case with a very small gap spacing, $s/D = 0.05$, for which there is a weak flow between the cylinders. The flow through the passage displaces, to a small degree, the two attached vortices towards the downstream. The flow is attached along both cylinders and there is a stagnation point in the flow along the midline between the cylinders, like what is shown in Fig. 5b. The length of the "detached vortices" is tremendously larger than that of an isolated single cylinder at the same Reynolds number. As shown in Fig. 6a, there is no separation region formed around the cylinders close to the gap, either upstream or downstream, when $s/D = 0.05$. For smaller gap spacings, e.g. $s/D = 0.005$, the flow resembles the flow in a corner and separation regions form around the gap both upstream and downstream of the cylinders. Maintaining the same gap spacing, increasing the Reynolds number increases the separation bubble length drastically, e.g. at Re = 20 Taneda's experiments on a single cylinder show a separation bubble of length $L_{SB} = 0.85D$ [23], whereas our simulation for two side-by-side cylinders with $s/D = 0.05$ gives $L_{SB} = 6.35D$. Hence, the side-by-side arrangement causes a separation bubble length much larger than that created by a cylinder of twice the diameter.

To investigate this observation a bit further, a comparison between the flow around two nearly-touching side-by-side cylinders and a flat plate normal to the flow is made in Fig. 7. Fig. 7a shows the flow streamlines around cylinders with the gap spacing $s/D = 0.05$ at Re = 20 (Re is based on the diameter of one cylinder). The Reynolds number based on the overall height, H, of the cylinder pair ($H = 2D + s$) is $\mathrm{Re}_H = 41$. The streamlines of the flow normal to a flat plate with height $H = 2D + s$, and thickness $0.025D$ were also computed at the same $\mathrm{Re}_H = 41$ (Fig. 7b). The separation bubble length for a single cylinder of diameter H, for two cylinders with $s/D = 0.05$, and for a flat plate normal to the flow, all at $\mathrm{Re}_H = 41$, are respectively $2.1H$, $3.1H$, and $5.2H$. One reason the flat plate has the most elongated vortex pair is that separation occurs at the corners of the plate, while this happens after the shoulders of the cylinders. A related reason is that greater pressure recovery in the wake of single cylinder and side-by-side cylinder pair reduces the radius of curvature of the separating streamline and therefore limits the separation bubble length.

As the gap spacing is increased to $s/D = 0.2$, the gap flow is enhanced, which pushes the twin vortices downstream. Relative to the smaller gap case, the separation bubble maintains its shape but its length varies slightly depending on the Reynolds number: at Re = 5, $L_{SB} = 1.25D$ for $s/D = 0.05$ and $L_{SB} = 1.15D$ for $s/D = 0.2$; at Re = 20, $L_{SB} = 6.35D$ for $s/D = 0.05$ and $L_{SB} = 7.05D$ for $s/D = 0.2$ (Fig. 8(b1) and (b2)).

For Re = 5, as the gap spacing is increased above $s/D = 0.2$, the gap flow is further strengthened and the two vortices shrink and are washed downstream (Fig. 8(a4)). When the gap spacing reaches $s/D = 0.5$, the vortices cease to exist and only a residual "bulge" is left in their place. The disappearance of the vortices is delayed and is more abrupt when the Reynolds number is increased, e.g. at Re = 20, this happens around $s/D \approx 0.6$.

There is a range of gap sizes (e.g., Fig. 8(a5)–(b5)) for which no vortices are present in the flow, even for Re = 20. In these cases, the gap flow resembles the flow in a channel with a sudden expansion.

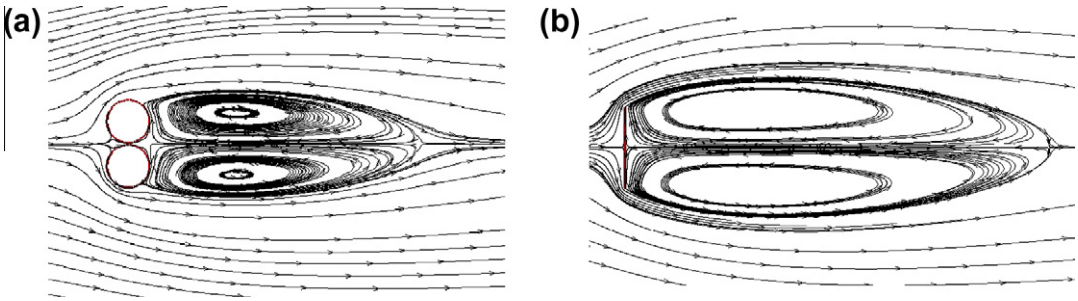

Fig. 7. (a) Flow around 2 side-by-side cylinders with $s/D = 0.05$ at Re = 20. The Reynolds number based on the overall height ($H = 2D + s$) is $Re_H = 41$. (b) A flat plate of height H normal to the flow at $Re_H = 41$. The plate thickness is $0.01H$.

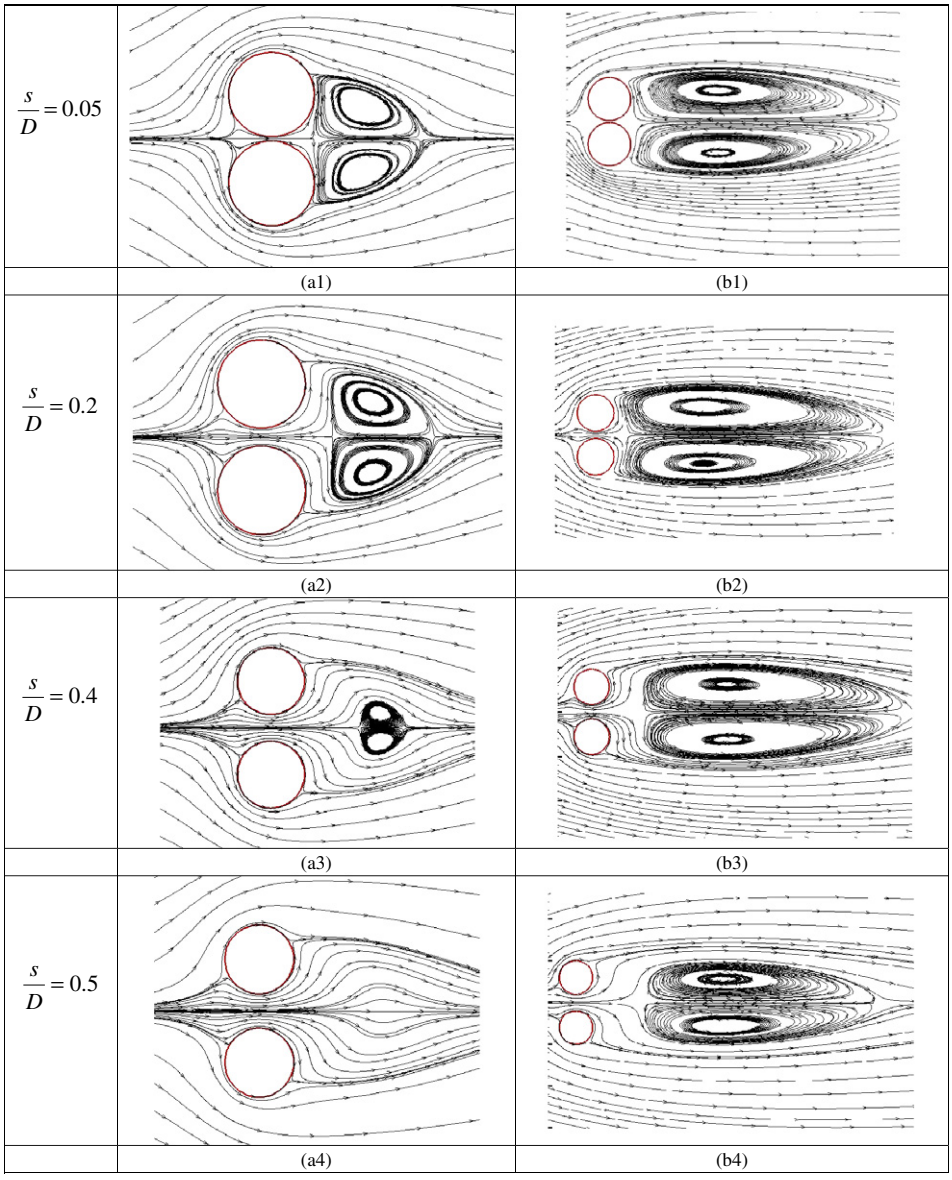

Fig. 8. Steady flow around two equal side-by-side cylinders at different Reynolds numbers and different gap spacings. The left column corresponds to Re = 5 and the right column to Re = 20.

As the gap size is increased still further, the cylinder flow starts to resemble the flow around isolated cylinders. At Re = 20 for $s/D \approx 1$ (Fig. 8(b6)), a small separation bubble is formed on the inner side of the cylinders. Increasing the gap spacing causes flow separation on the outer side of the cylinders as well, i.e. a return to twin-vortex formation behind each cylinder, but the flow regime is asymmetrical about each cylinder owing to the streamline expansion caused by losses in the gap flow (Fig. 8(b7)–(b8)).

The streamlines of the initial twin vortices flow regime, Fig. 8(b4), are quite different than the streamlines of the sudden

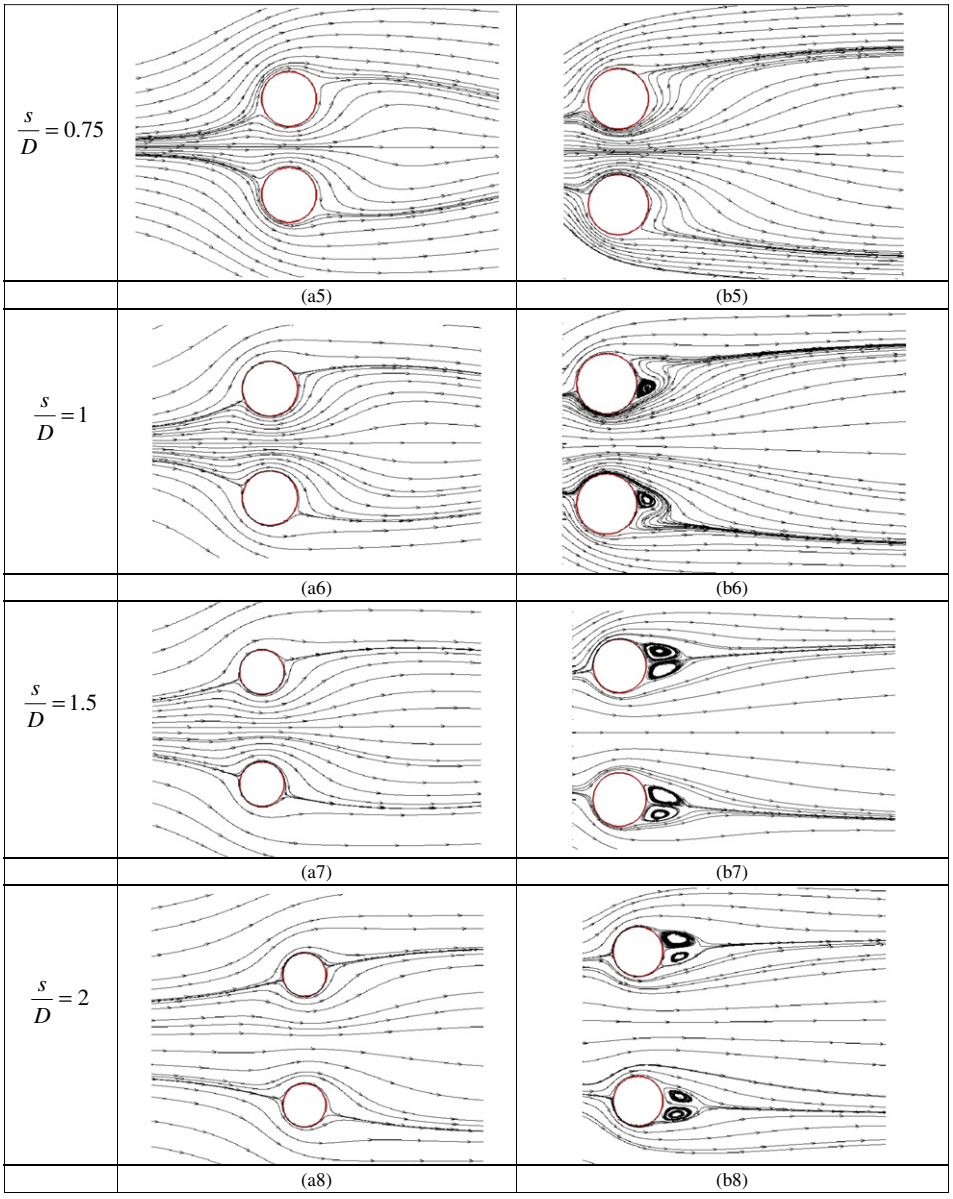

Fig. 8 (*continued*)

expansion flow regime, Fig. 8(b5). The difference in the streamlines is a bit deceptive. As the gap increases from $s/D = 0.5$ to $s/D = 0.75$, there is a smooth transition from a slightly negative axial velocity along the centerline to a slightly positive one (e.g. refer to Fig. 9 for the velocity distributions at $x/D = 5$).

3.2. Stagnation/separation points

Fig. 10 shows the front stagnation point location as a function of the gap spacing, with Reynolds number as the parameter. As the gap spacing increases the front stagnation point approaches asymptotically the position for an isolated cylinder, $\theta_f = 90°$. At higher Reynolds numbers the approach towards the asymptotic limit is steeper, owing to the dominant effects of the inertial forces at higher Re.

Fig. 11 shows the change in the rear stagnation point position with the gap spacing for low Reynolds numbers. For Re = 1 and Re = 5 the rear stagnation point angle first increases with s/D, reaches a peak, and then asymptotically approaches 90° at large values of s/D.

The singular points at Re = 20 are shown separately in Fig. 12. Up to $s/D \approx 1$, there is only a slight change in the rear stagnation point. Interestingly, the dynamical behavior of the flow trifurcates for $s/D > 1$. For gap spacings in the range $1 < s/D < 1.5$, a separation region forms on the inner side of the cylinder, as shown in Fig. 6b. This creates a reattachment point and a separation point on the rear side of the cylinders. For gap spacings $s/D > 1.5$, the asymmetrical pair of vortices reform to produce an upper and a lower separation point together with the reattachment point, see Fig. 8(b7) and (b8). The angular positions of these singular points are almost fixed for different values of the gap spacing.

3.3. Drag and lift coefficients

The trend in the lift and drag coefficients for these moderate Reynolds numbers is different than occurs at higher Reynolds numbers. For comparison purposes we ran time-dependent CFD simulations at Re = 100, at which Reynolds number vortex streets are shed into the flow. The time-averaged lift and drag coefficients

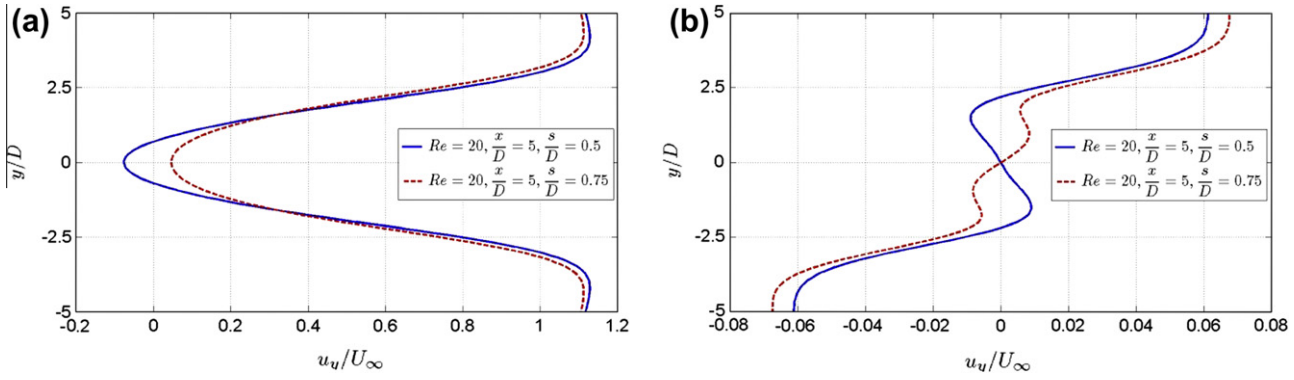

Fig. 9. A comparison of (a) x-component (b) y-component of velocity between Fig. 8(b4) and (b5) corresponding to gap spacings $s/D = 0.5$ and $s/D = 0.75$ at Re = 20.

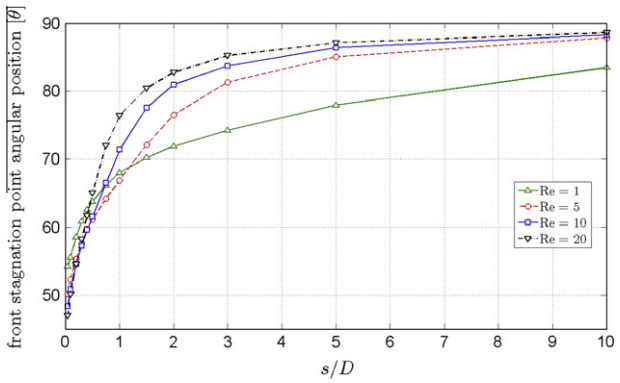

Fig. 10. Front stagnation point angular position versus gap spacing with Re as the parameter.

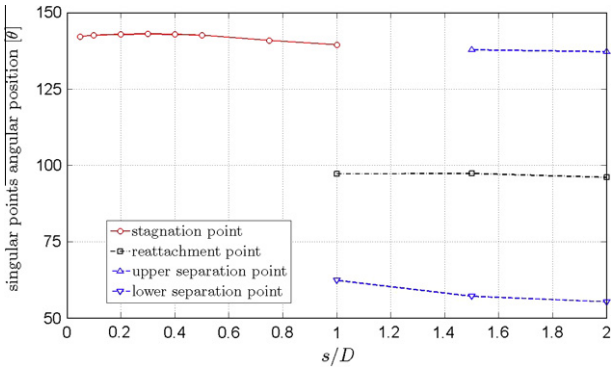

Fig. 12. Angular position of rear stagnation/separation/reattachment points versus gap spacing at Re = 20. Note that for $1 < s/D < 1.5$ a counter-rotating vortex pair forms in the wake of the cylinders.

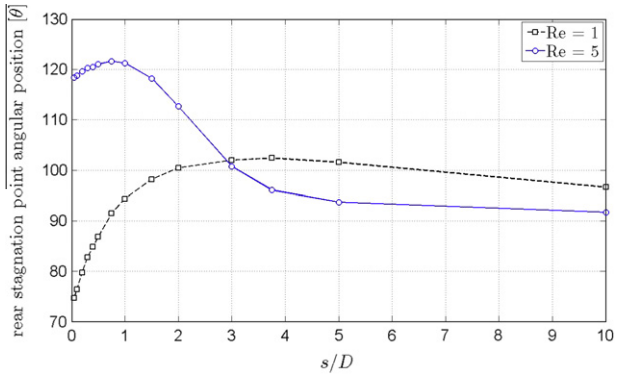

Fig. 11. Rear stagnation point angular position versus gap spacing with Re as parameter.

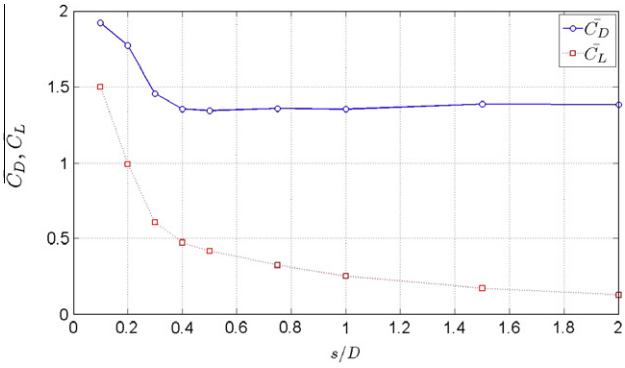

Fig. 13. Time-averaged lift and drag coefficient of two side-by-side cylinders versus gap spacing at Re = 100.

of these simulations are presented in Fig. 13. These results are in good agreement with those presented in [18]; at Re = 100 and $s/D = 0.2$, Kang gives $\overline{C}_L = 1.04$ and we calculated $\overline{C}_L = 0.99$. The lift coefficient should approach zero when the gap spacing is increased. As seen in Fig. 13 there is a monotonic decrease in the lift coefficient with gap spacing. This trend in lift resembles that of a single cylinder placed near a wall in a shear-free flow [26,27]. At small gap spacings the drag coefficient is greater than that of a single cylinder in the flow and then it is almost constant for $s/D > 1.5$. At the low to moderate Reynolds numbers that are the focus of this article, almost none of the higher Reynolds number trends are observed, as explained below.

Variations of the drag coefficient with the gap spacing for different Reynolds numbers, $1 \leqslant \mathrm{Re} \leqslant 20$, are depicted in Fig. 14. In contrast with the increased drag of cylinders in proximity, shown in Fig. 13, at these lower Reynolds numbers there is a pronounced reduction in the drag coefficient for small gap spacings.

Fig. 15 shows the contribution of the viscous drag and pressure drag to the total drag for different gap spacings at Re = 20. As is clear in Fig. 15, the primary reason for the reduced drag of cylinders in close proximity is the reduced viscous drag, not any marked change in the overall pressure drag.

The variation of the lift coefficient with the gap spacing is much more complicated than the drag coefficient, as shown in Fig. 16. For Reynolds numbers $\mathrm{Re} \leqslant 10$, there is an initial increase in the lift coefficient as s/D increases, it reaches a maximum, and then asymptotically decreases to zero. At Re = 1 this peak lift happens at larger values of s/D than for Re = 5. For example this point is

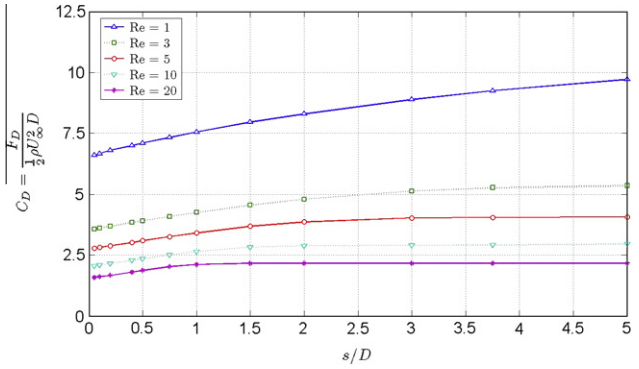

Fig. 14. Drag coefficient of the side-by-side cylinders versus gap spacing with Re as a parameter.

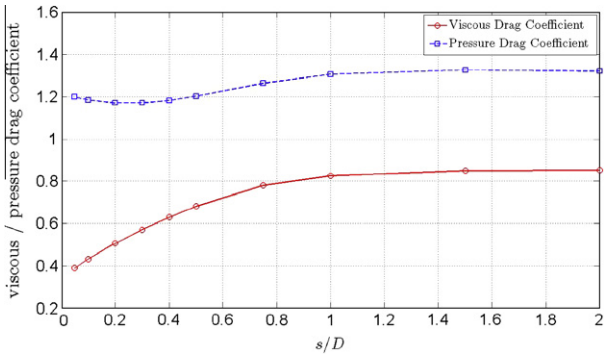

Fig. 15. Variation of the viscous and pressure drag coefficients with s/D at Re = 20 for two cylinders side-by-side in a cross flow.

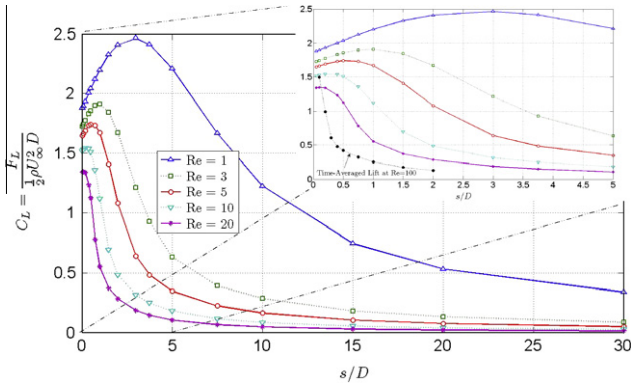

Fig. 16. Lift coefficient of the side-by-side cylinders versus gap spacing with Re as a parameter.

around $s/D \approx 1$ at Re = 3, whereas it occurs around $s/D \approx 0.7$ at Re = 5. The lift coefficient curve is sigmoidal. The curve is concave down for small s/D, has a point of inflection, and then is concave up and asymptotes to the x-axis when the cylinders are far apart. The inflection point moves towards a smaller gap spacing as the Reynolds number increases, as expected. For comparison with higher Reynolds number flows, the time-averaged lift coefficient at Re = 100 is also shown on the graph.

3.3.1. Numerical fit to lift and drag coefficients

The numerically computed drag and lift coefficients were parameterized as functions of Re and separation distance. Our initial emphasis was on the role of the separation distance and

Table 2
Drag coefficient curve fit.

$C_D(x, \mathrm{Re}) = d_1 erf(d_2 x) + d_3 \frac{x+d_4}{x+d_5}$

$d_1 = 3.35(\mathrm{Re}^{-0.40}) - 0.363$
$d_2 = 0.16(\mathrm{Re}^{0.64}) + 0.017$
$d_3 = 6.65(\mathrm{Re}^{-0.87}) + 1.052$

$x = \frac{s}{D}$

$d_4 = 1.35(\mathrm{Re}^{-1.61}) - 0.010$
$d_5 = 1.58(\mathrm{Re}^{-1.76}) + 0.012$

Table 3
Lift coefficient curve fit.

$C_L(x, \mathrm{Re}) = \frac{l_1 x^2 + l_2 x + l_3}{x^4 + l_5}$

$l_1 = 3.05(\mathrm{Re}^{-0.78} + 0.092) erf(0.165\mathrm{Re}^{1.6})$
$l_2 = 25.02(\mathrm{Re}^{-1.93}) - 0.28$
$l_3 = 133.90(\mathrm{Re}^{-1.72}) - 1.15$

$x = \frac{s}{D}$

$l_4 = -0.67(\mathrm{Re}^{-0.67}) + 3.13$
$l_5 = 71.84(\mathrm{Re}^{-1.65}) - 0.72$

Table 4
Maximum and rms difference of drag and lift coefficient between simulations and curve fit.

Re	Drag coefficient		Lift coefficient	
	Maximum diff. (%)	RMS diff. (%)	Maximum diff. (%)	RMS diff. (%)
1	0.9	0.4	3.9	1.0
3	4.2	1.9	6.2	2.6
5	8.9	4.2	8.9	4.2
10	16	7.9	7.8	4.7
20	16.5	9.7	15.7	9.7

we then considered the effect of Reynolds number. For a fixed Re we used the optimization toolbox in MATLAB (nonlinear curve-fitting in the least-squares sense) to find functional fits to the simulation results. The coefficients of the parameters in the functional fits were then made functions of Re, and these functions were in turn determined by least-squares fitting to simulation results at several Re. In total, seven different Reynolds numbers and 14 separation distances were used to obtain the drag and lift coefficient correlations.

The reduced drag on the cylinders (Fig. 14) is well represented by a combination of two functions; an error function and a rational function (Table 2). The root mean square (rms) deviation between the cylinders' drag predicted by the curve fit and from simulations is 6%, when averaged over all cylinder separations and Reynolds numbers. For a given Reynolds number, the maximum difference and rms difference calculated for all gap spacings are tabulated in Table 4. The maximum differences occur at small gap spacings.

The non-monotonic dependence on s/D of the lift coefficient of cylinders makes that lift difficult to parameterize. Apart from the range $15 < \mathrm{Re} < 20$, the cylinders' lift coefficient is well fit by a

rational function (Table 3); with the numerator a quadratic function and the denominator a power law. The function fit may be used for $15 < Re < 20$, but only for $s/D > 5$. The rms deviation between the cylinders' lift coefficient predicted by the curve fit and from simulations is 4.3%. The maximum and rms difference between simulations and curve fits of lift for all gap spacings are tabulated in Table 4.

4. Conclusions

Computer simulations of the flow around two-dimensional side-by-side circular cylinders, at low to moderate Reynolds numbers, have been conducted to investigate the effect of the gap spacing between the cylinders on the lift and drag coefficients. The gap spacing is varied in the range $0.05 < s/D < 30$, and Reynolds numbers between 1 and 20 were studied.

For very small gap spacing, two elongated "detached vortices" form downstream of the cylinders. Increasing the Reynolds number increases the separation bubble length drastically. The small gap ratios, e.g. $0.2 < s/D < 0.4$ for $Re = 5$ and $0.4 < s/D < 0.6$ for $Re = 20$, is characterized by the shrinkage of the two vortices, accompanied by the disappearance of them around $s/D \approx 0.5$ for $Re = 5$ and $s/D \approx 0.6$ for $Re = 20$. For intermediate gap sizes, e.g. $s/D \approx 2$ at $Re = 10$ and $s/D \approx 1$ at $Re = 20$, the cylinder flow starts to resemble the flow around isolated cylinders, but only one small separation bubble forms on the inner side of the cylinders. For larger values of gap spacing twin vortices form behind each cylinder, but the flow streamlines around each cylinder are asymmetrical. In addition, the front stagnation point approaches asymptotically the position for an isolated cylinder, $\theta_f = 90°$, as the gap spacing increases.

The variation of the lift and drag coefficients for these moderate-Reynolds-number flows is different than occurs at higher Reynolds numbers. At small gap spacings the drag coefficient is considerably smaller than that of a single cylinder. The reduction in the drag is attributable to the reduced viscous drag at small gap spacing. The variation of the lift coefficient with the gap spacing follows a sigmoidal pattern: for small s/D it is concave down, and then it is concave up to asymptotically approach the x-axis when s/D is large. Curve fits of $C_L\left(\frac{s}{D}, \mathrm{Re}\right)$ and $C_D\left(\frac{s}{D}, \mathrm{Re}\right)$ are provided.

Acknowledgments

The authors are grateful for the financial support provided by AstenJohnson Inc. and the Natural Sciences and Engineering Research Council of Canada.

References

[1] Vakil A, Green SI. Drag of tandem circular cylinders at moderate reynolds numbers – two dimensional flow. Theoretical and Computational Fluid Dynamics; submitted for publication.
[2] Zdravkovich MM. Flow around circular cylinder. Fundamentals, vol. 1. Oxford University Press; 1997.
[3] Zdravkovich MM. Flow around circular cylinder. Applications, vol. 2. Oxford University Press; 2003.
[4] Young EWK, Martinex DM, Olson JA. The sedimentation of papermaking fibers. Am Inst Chem Eng 2006;52:2697–706.
[5] Taneda S. Experimental studies of the lift of two equal circular cylinders placed side by side in a uniform stream at low Reynolds numbers. J Phys Soc Jpn 1957;12:419–22.
[6] Fujikawa H. The forces acting on two equal circular cylinders placed in a uniform stream at low values of Reynolds number. J Phys Soc Jpn 1956;11:558–69.
[7] Taneda S. Visualization of Separating stokes flows. J Phys Soc Jpn 1979;46:1935–42.
[8] Umemura A. Matched-asymptotic analysis of low-Reynolds-number flow past two equal circular cylinders. J Fluid Mech 1982;121:345–63.
[9] Zdravkovich MM. Review of flow interference between two circular cylinders in various arrangements. Trans ASME: J Fluids Eng 1977:618–33.
[10] Ishigai S, Nishikawa E, Nishimura K, Cho K. Experimental study on structure of gas flow in tube banks with tube axis normal to flow. Bull JSME 1972;15:949–56.
[11] Bearman PW, Wadcock AJ. The interaction between a pair circular cylinders normal to a stream. J Fluid Mech 1973;61:499–511.
[12] Zdravkovich MM. Interaction of bistable/metastable flows and stabilizing devices. In: Bearman PW, editor. Proceedings of the 6th international conference on flow-induced vibrations. Rotterdam: Balkema; 1995. p. 431–9.
[13] Norberg C. An experimental investigation of the flow around a circular cylinder: influence of aspect ratio. J Fluid Mech 1994;258:287–346.
[14] Norberg C. Flow around a circular cylinder: aspect of fluctuating lift. J Fluids Struct 2001;15:459–69.
[15] Norberg C. Fluctuating lift on a circular cylinder: review and new measurements. J Fluids Struct 2003;17:57–96.
[16] Inoue Q, Sakuragi A. Vortex shedding from a circular cylinder of finite length at low Reynolds numbers. Phys Fluids 2008;20:033601–12.
[17] Williamson CHK. Evolution of a single wake behind a pair of bluff bodies. J Fluid Mech 1985;159:1–18.
[18] Kang S. Characteristic of flow over two circular cylinders in a side-by-side arrangement at low Reynolds numbers. Phys Fluids 2003;15:2486–98.
[19] Ng CW, Ko NWM. Flow interaction behind two circular cylinders of equal diameter – a numerical study. J Wind Eng Ind Aerodynam 1995;54/55:277–87.
[20] Xu SJ, So RMC. Reynolds number effects on the flow structure behind two side-by-side cylinders. Phys Fluids 2003;15:1214–9.
[21] Meneghini JR, Saltara F, Siqueira CLR, Ferrari JA. Numerical simulation of flow interference between two circular cylinders in tandem and side-by-side arrangements. J Fluids Struct 2001;15:327–50.
[22] Peschard I, LeGal P. Coupled wakes of cylinders. Phys Rev Lett 1996;77:3122–5.
[23] Taneda S. Experimental investigation of the wake behind cylinders and plates at low Reynolds numbers. J Phys Soc Jpn 1956;11:302–7.
[24] Fornberg B. A numerical study of steady viscous flow past a circular cylinder. J Fluid Mech 1980;98:819–55.
[25] Sen S, Mittal S, Biswas G. Steady separated flow past a circular cylinder at low Reynolds numbers. J Fluid Mech 2009;620:89–119.
[26] Fredsøe J, Hansen EA. Lift forces on pipelines in steady flow. J Waterway, Port, Coastal, Ocean Eng, ASCE 1987;113(2):139–55.
[27] Fredsøe J, Sumer BM, Andersen J, Hansen EA. Transverse vibrations of a cylinder very close to a plane wall. J Offshore Mech Arct Eng 1987;109(1):52–60.